Electrochemistry Communications 87 (2018) 66–70

Contents lists available at ScienceDirect

Electrochemistry Communications

journal homepage: www.elsevier.com/locate/elecom

$NiCo_2O_4$ nanowires@MnO_x nanoflakes supported on stainless steel mesh with superior electrocatalytic performance for anion exchange membrane water splitting

L. Zeng[a,b], T.S. Zhao[a,*], R.H. Zhang[a], J.B. Xu[a]

[a] Department of Mechanical and Aerospace Engineering, The Hong Kong University of Science and Technology, Clear Water Bay, Kowloon, Hong Kong, China
[b] HKUST Jockey Club Institute for Advanced Study, The Hong Kong University of Science and Technology, Clear Water Bay, Kowloon, Hong Kong, China

ARTICLE INFO

Keywords:
Water splitting
$NiCo_2O_4$ nanowires
MnO_x nanoflakes
Core-shell structure
Electrocatalytic activity

ABSTRACT

A core-shell structured catalyst with $NiCo_2O_4$ nanowires as the core and MnO_x nanoflakes as the shell is synthesized and deposited on a stainless steel mesh, and applied in anion exchange membrane water splitting. This unique structured catalyst allows the core material, $NiCo_2O_4$ nanowires, to serve as the electrically conductive skeleton, and the shell material, MnO_x nanoflakes, to be the electroactive sites. As a result, the catalyst exhibits a superior electrocatalytic activity (η = 342 mV @10 mA cm^{-2}) toward the oxygen evolution reaction. The water splitting cell with the catalyst can be operated at 200 mA cm^{-2} with an overpotential of about 500 mV and stably run for 100 h without significant degradation. The results demonstrated here shows that the $NiCo_2O_4$@MnO_x is a promising candidate for the oxygen evolution reaction in the alkaline media.

1. Introduction

Recently, anion exchange membrane (AEM) water splitting has been developed to address the cost issue related to its counterpart, proton exchange membrane water splitting [1–3]. Although the alkaline environment permits the employment of non-precious catalysts as the catalyst for oxygen evolution reaction (OER), the rational design of an efficient electrode with high electroactivity and excellent stability is still a critical challenge for AEM water splitting [4–6]. As one of the most promising alternatives, novel catalysts based on the transition metal oxides (TMOs) with different compositions and morphologies are widely explored. Among these TMOs, $NiCo_2O_4$ has been extensively studied as the catalyst for OER, owing to its superior electrical conductivity, abundant and tunable active sites [7–9].

Meanwhile, the $NiCo_2O_4$ serves as the skeleton to deposit other nanostructured catalysts, such as Co_3O_4/$NiCo_2O_4$ [10], graphene nanosheets/$NiCo_2O_4$ [11] and Au/$NiCo_2O_4$ [12], has been recently proposed to further improve the electrocatalytic activity. Even though there are some promising results based on the $NiCo_2O_4$ have been achieved, the overpotentials at a current density of 10 mA cm^{-2}, which is a metric relevant to solar fuel synthesis, in these composite catalysts are still high, which restricts the application of these catalysts in the AEM water splitting.

To address this issue, we electrochemically deposited MnO_x nanoflakes (NFs) on the $NiCo_2O_4$ nanowires (NWs)-decorated stainless steel (SSL) mesh and explored its electrocatalytic activity toward the OER in the alkaline media for the first time. The MnOx was chosen due to the nanostructured manganese oxides have been shown as a superior catalyst for the OER in the alkaline media [13]. The superior electrocatalytic activity was not only demonstrated in the three-electrode-cell system but also verified in an AEM water splitting cell.

2. Experimental

2.1. Synthesis of $NiCo_2O_4$@MnO_x supported on SSL mesh

A twill-woven stainless steel mesh (SSL mesh, #600) was selected as the supporting layer. The self-supported $NiCo_2O_4$ NWs on the SSL mesh were prepared as reported elsewhere [14]. The mass loading was 0.5 mg cm^{-2}. After that, MnO_x NFs were fabricated on $NiCo_2O_4$ NWs by an electrodeposition process in a conventional three-electrode cell [15]. The deposition was performed in a solution containing 0.1 M manganese acetate and 0.1 M ammonium acetate. The $NiCo_2O_4$/SSL was vertically submerged into the solution as the working electrode. Pt mesh and Ag/AgCl (3.5 M KCl) were used as the counter electrode and reference electrode, respectively. The MnO_x precursors were deposited galvanostatically with a current density of 2 mA cm^{-2} and then annealed at 300 °C in ambient air for 1 h to obtain $NiCo_2O_4$@MnO_x/SSL.

* Corresponding author.
E-mail address: metzhao@ust.hk (T.S. Zhao).

https://doi.org/10.1016/j.elecom.2018.01.002
Received 3 December 2017; Received in revised form 26 December 2017; Accepted 4 January 2018
Available online 05 January 2018

The mass loading of MnO_x was 0.6 mg cm^{-2}.

2.2. Material characterizations

Transmission electron microscopy (TEM) images were obtained by operating a high-resolution JEOL 2010F TEM system with a LaB_6 filament at 200 kV. Surface morphology was determined by a field-emission scanning electron microscope (FESEM, JEOL 6700F). The X-ray diffraction (XRD) pattern was analyzed with a Philips high-resolution X-ray diffraction system (model PW 1825) using a Cu Kα source operating at 40 kV with the scan rate of 0.025° s^{-1}. The X-ray photoelectron spectroscopy (XPS) characterization was determined by a Physical Electronics PHI 5600 multi-technique system using Al monochromatic X-ray at a power of 350 W. Raman measurements were performed with an RM3000 (Renishaw) micro-Raman spectrometer at 514.5 nm. The laser beam was focused onto the sample with a 50 × objective.

2.3. Electrochemical measurements

The electrochemical activity was investigated by linear sweep voltammetry (LSV) that implemented with the same three-electrode cell as described above. The samples were subjected to electrochemical treatment by potential scanning from 0 to + 0.70 V vs. Ag/AgCl in 0.1 M KOH. The electrolyte was saturated with oxygen by bubbling oxygen gas at least 30 min in advance. A home-made IrO_2/C (10 wt%) was employed as the benchmark for OER process. The IrO_2/C with a mass loading of 0.2 mg cm^{-2} was brushed on the SSL mesh with a home-made ionomer as the binder.

2.4. AEM water splitting

The AEM water splitting was evaluated in a home-made water electrolysis setup. The membrane with a thickness of 60 μm was cast with the home-made ionomer suspension. The as-fabricated samples were directly employed as the electrode for OER (5 pieces) while a commercial powder catalyst (Acta 4030) was employed as the electrode for hydrogen evolution reaction (HER). The HER catalyst loading in the as-prepared electrode was 4 mg cm^{-2}. The performance of IrO_2/C supported SSL mesh was also evaluated for the purpose of comparison. The fabrication procedure of membrane-electrode-assemblies (MEAs) and test protocol were the same as reported in our previous work [16]. All measurements were performed at 60 °C.

3. Results and discussion

A typical low-resolution SEM image (inset of Fig. 1a) illustrates that the entire surface of the bare SSL mesh is densely covered with $NiCo_2O_4$ NWs. A high-resolution SEM image (Fig. 1a) reveals that $NiCo_2O_4$ NWs with a hexagonal cylinder architecture are radially grown on the SSL mesh with a length of 0.5–4 μm and an average diameter of 50 nm. It is also clearly observed that the mesopores emerge in the $NiCo_2O_4$ NWs due to the stacking of small nanoparticles (5–20 nm). The interconnected mesopores will be beneficial for the accessibility to electrolyte and oxygen, enabling full utilization of the electroactive surface area of NWs and fast electronic, ionic transportation through the electrode. Subsequently, MnO_x NFs are electrodeposited galvanostatically on $NiCo_2O_4$ NWs followed by a thermal treatment process. As presented in Fig. 1b–c, the surface of $NiCo_2O_4$ NWs is completely deposited by various MnO_x NFs with distinct folds (thickness: 3–9 nm) due to the highly electrical and electrochemical active property of $NiCo_2O_4$ NWs. Meanwhile, thanks to the weak alkaline electrolyte, the mesoporous structure of $NiCo_2O_4$ NWs is persevered after the electrodeposition process, as confirmed by a typical TEM image (Fig. 1d). Typical HRTEM image (Fig. 1e) shows that clear lattice fringes with interfringe distances of approximately 2.52 Å and 2.76 Å, corresponding to the (311) and (220) plane of the spinel phase $NiCo_2O_4$. Then, the selected area electron diffraction measurement was performed (not shown), and the result indicates that $NiCo_2O_4$ NWs possessed a polycrystalline structure. Meanwhile, typical HRTEM image presented in Fig. 1f shows that as-fabricated MnO_x NFs possess a nonuniform microcrystalline structure.

The crystallinity of as-prepared samples is determined by XRD (Fig. 2a). The strong diffraction peaks, locating at 43.4°, 50.6° and 74.5°, are derived from the SSL mesh while other diffraction peaks emerged in the $NiCo_2O_4$/SSL sample, can be readily indexed as spinel $NiCo_2O_4$ phase (JCPDS card No. 073-1702). After fabricated with MnO_x NFs, no new peaks are visible in the $NiCo_2O_4$@MnO_x/SSL sample apparently, suggesting that MnO_x NFs exist as an amorphous or weak-crystallinity structure in the composite nanostructure, as confirmed by HRTEM. It should be noted that Mn_2O_3 is the best phase of MnO_x for the OER [15,17]. However, the transfer from MnOOH to Mn_2O_3 requires a thermal treatment at 500 °C in the ambient air, in which process the morphology of $NiCo_2O_4$ is completely collapsed. This is the reason why we thermally implemented the conversion at relatively low temperature. Actually, the MnO_x can be partially converted to Mn_2O_3 by the subsequently electrochemical measurement [13].

The surface elemental compositions are further investigated by XPS. The raw Co 2p spectrum of $NiCo_2O_4$/SSL can be deconvoluted into two peaks that are assigned to Co^{3+} (779.3 eV for Co $2p_{3/2}$) and Co^{2+} (780.8 eV), and one shakeup satellite (Fig. 2b). The raw Ni 2p spectrum of $NiCo_2O_4$/SSL can be also deconvoluted into two peaks that are assigned to Ni^{2+} (854.2 eV for Ni $2p_{3/2}$) and Ni^{3+} (855.8 eV), and one shakeup satellite (not shown). The ratio of Co^{2+}/Co^{3+} and Ni^{3+}/Ni^{2+} calculated from the fitted area are 1.20 and 2.22, respectively. It was reported that high ratio of Co^{2+} and Ni^{3+} contributed to the superior electrocatalytic activity for OER in the alkaline media [18,19]. Meanwhile, after the electrodeposition of MnO_x NFs, the entire surface of $NiCo_2O_4$ NWs is covered by MnO_x NFs since the peaks are disappeared in the Co 2p spectrum of $NiCo_2O_4$@MnOOH/SSL. Simultaneously, the raw Mn 2p spectrum emerges in the $NiCo_2O_4$@MnO_x/SSL sample and can be fitted with two peaks: Mn^{3+} species (641.8 eV for Mn $2p_{3/2}$) and Mn^{4+} species (642.9 eV). There is also a satellite peak in the deconvolution spectrum of Mn 2p.

High electronic conductivity is also important for OER catalysts since the OER occurs on the electrode surface and the generated electrons thereafter need to be transferred. The electrical resistance of as-prepared samples is measured in a self-designed cell. From the I-V curve as presented in Fig. 2d, it is observed that the deposition of nanostructured catalysts slightly increases the area resistances, which is still acceptable for practical application.

The electrochemical activity is measured by polarization curves, as shown in Fig. 3a. Due to the SSL mesh exhibits a poor activity toward OER process, the influence from the conductive substrate can be eliminated. In both $NiCo_2O_4$/SSL and $NiCo_2O_4$@MnO_x/SSL, there exists a Co(III)/Co(IV) redox peak in prior to the OER process. While after being deposited with MnO_x NFs, the onset potential for the OER is significantly negative-shifted, which indicates the MnO_x NFs contribute to the increased OER activity. Thus, to reach the same current density of 10 mA cm^{-2}, the overpotential for $NiCo_2O_4$@MnO_x/SSL is 342 mV, which is lower than that of overpotential for $NiCo_2O_4$/SSL (386 mV). Although the overpotential of $NiCo_2O_4$@MnO_x/SSL is still much larger than that of overpotential for IrO_2/C (221 mV), our freestanding electrode outperforms other integrated electrodes [7,20] and $NiCo_2O_4$-based hybrid catalysts [8,21] for the OER. The corresponding Tafel plots derived from LSV curves are plotted in Fig. 3b to gain further insight into the OER activity. Apparently, the overpotential for $NiCo_2O_4$@MnO_x/SSL is around 50 mV lower than that of $NiCo_2O_4$/SSL at the same current density. Simultaneously, the Tafel slope of $NiCo_2O_4$@MnO_x/SSL is 64 mV dec^{-1}, compared to 73 mV dec^{-1} for $NiCo_2O_4$/SSL. Since the Tafel slope relates to the reaction mechanism, the reduced Tafel slope indicates the effective charge-transfer and high

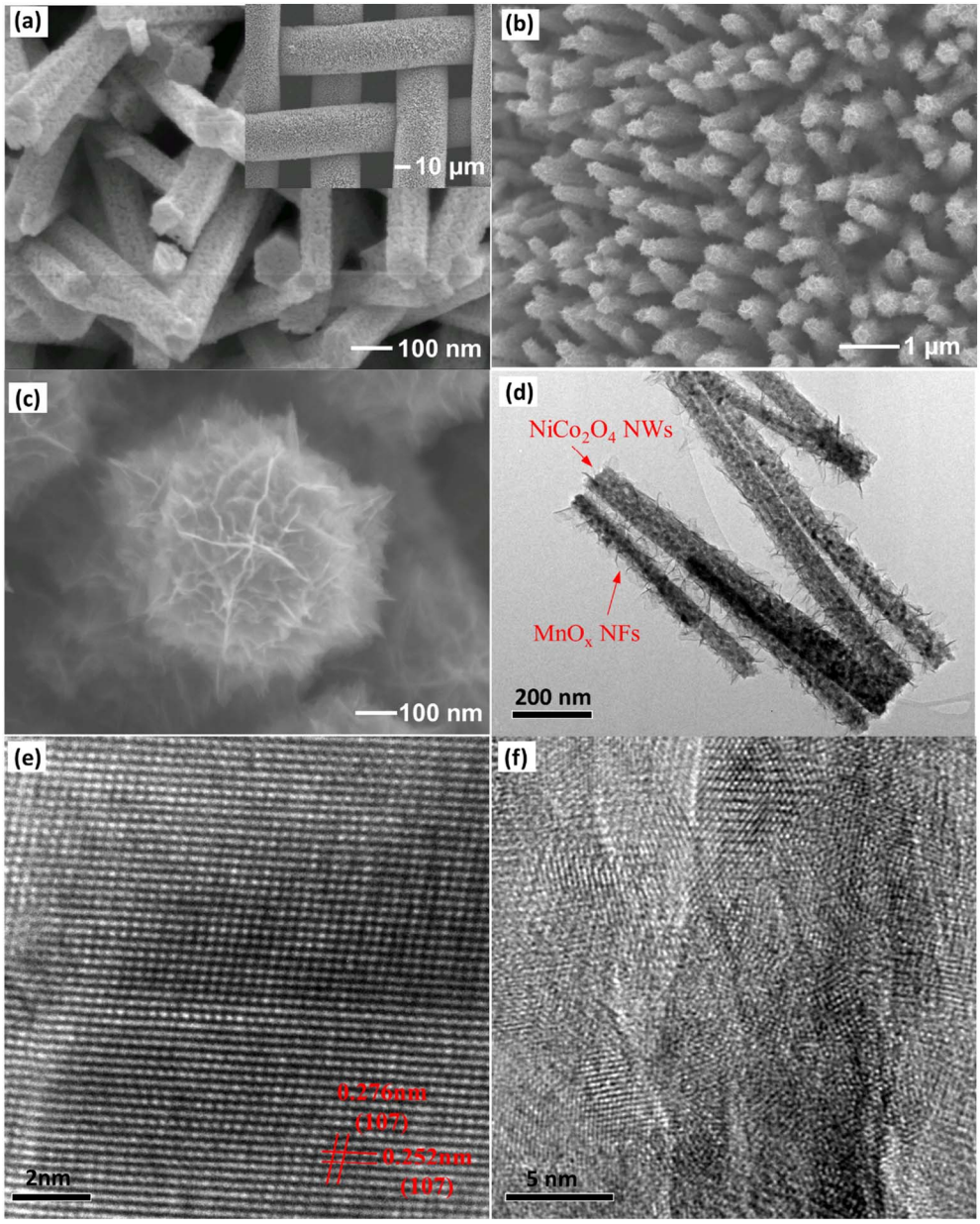

Fig. 1. Typical SEM images of $NiCo_2O_4$/SSL (a) and $NiCo_2O_4$@MnO_x/SSL (b–c); a low-resolution TEM image of $NiCo_2O_4$@MnO_x/SSL (d); high-resolution TEM images of $NiCo_2O_4$ (e) and MnO_x (f).

efficiency of $NiCo_2O_4$@MnO_x/SSL for OER. The Tafel slope of $NiCo_2O_4$@MnO_x/SSL is similar to the value obtained on IrO_2/C (58 mV), which is indicative of the similar reaction mechanism.

Finally, the catalysts are employed to fabricate MEA and evaluated the electrochemical activity for AEM water splitting. As shown in Fig. 3c, with the aid of MnO_x NFs, the activation loss in the cell with $NiCo_2O_4$@MnO_x/SSL as the catalyst is significantly reduced as compared with the cell with $NiCo_2O_4$/SSL. At a current density of 200 mA cm^{-2}, the applied voltage of the cell decreases from 1.79 V to 1.74 V when the MnO_x NFs are deposited on the $NiCo_2O_4$ NWs. The improvement of electrocatalytic performance can be attributed to the synergistic effect. That is, the $NiCo_2O_4$ NWs contribute to the porous and electrically conductive skeleton, and the MnO_x NFs contribute to the high electroactive sites as a result of the reduced activation barrier on the surface of MnO_x for the OER. Although the overpotential of the cell with $NiCo_2O_4$@MnO_x/SSL is still larger than that of the cell with IrO_2/C as the catalyst, the performance demonstrated here is competitive when compared with the performance reported in the literature [2,3]. Meanwhile, the electrode stability is determined by a continuous constant-current electrolysis (Fig. 3d). The cell voltage can be maintained at around 1.86 V at a current density of 400 mA cm^{-2} for 100 h. The internal resistance was periodically measured by AC impedance at a high frequency (1 kHz). The internal resistance stays at around 0.42 Ω cm^2, which indicates that the as-prepared electrode is stable during the continuous operation.

4. Conclusions

In summary, $NiCo_2O_4$@MnO_x was supported on the SSL mesh for the AEM water electrolysis. It was demonstrated that the deposition of MnO_x NFs on the surface of $NiCo_2O_4$ NWs significantly enhanced the electrocatalytic activity toward the OER. More importantly, the AEM water splitting with the $NiCo_2O_4$@MnO_x/SSL as the OER catalyst was operated at 200 mA cm^{-2} with an overpotential of about 500 mV and stably run for 100 h without significant degradation. These results suggest that the $NiCo_2O_4$@MnO_x can serve as a low-cost, high-performance catalyst for the OER in the alkaline environment.

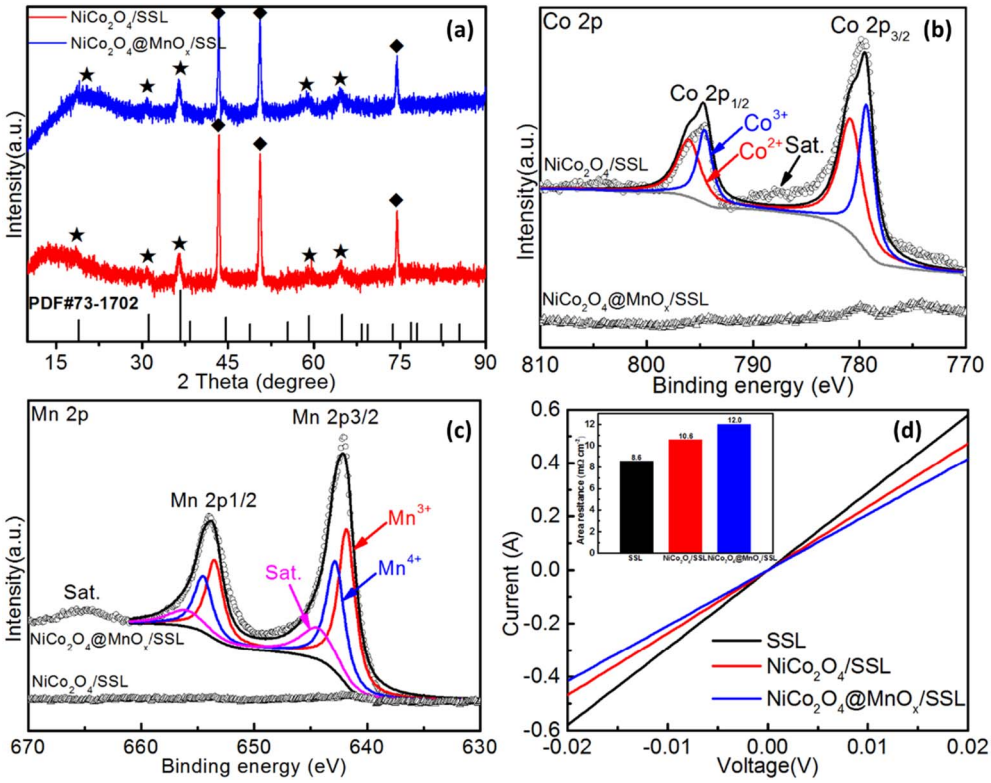

Fig. 2. The XRD patterns (a) of as-prepared samples. High-resolution XPS survey spectra for (b) Ni 2p; (c) Mn 2p; (d) area resistance measurement for different electrodes.

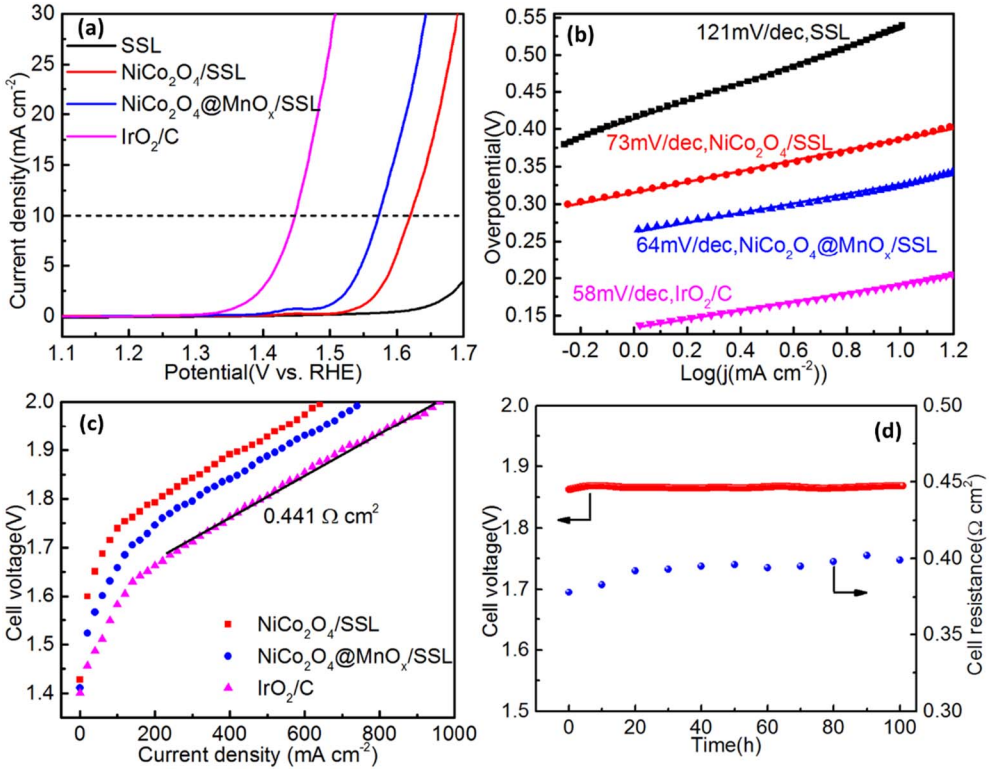

Fig. 3. The *iR*-corrected LSV curves and Tafel plots for different electrodes (a and b); AEM water electrolysis performance of MEAs with different electrodes (c); transient voltage and AC resistance of AEM water splitting with $NiCo_2O_4$@MnO_x/SSL as the electrode for OER (d).

Acknowledgements

The work described in this paper was fully supported by a grant from the Research Grants Council of the Hong Kong Special Administrative Region, China (Project No. 16200717).

References

[1] Y.J. Leng, G. Chen, A.J. Mendoza, T.B. Tighe, M.A. Hickner, C.Y. Wang, Solid-state water electrolysis with an alkaline membrane, J. Am. Chem. Soc. 134 (2012) 9054–9057.

[2] L. Xiao, S. Zhang, J. Pan, C.X. Yang, M.L. He, L. Zhuang, J.T. Lu, First implementation of alkaline polymer electrolyte water electrolysis working only with pure water, Energy Environ. Sci. 5 (2012) 7869–7871.

[3] C.C. Pavel, F. Cecconi, C. Emiliani, S. Santiccioli, A. Scaffidi, S. Catanorchi, M. Comotti, Highly efficient platinum group metal free based membrane-electrode assembly for anion exchange membrane water electrolysis, Angew. Chem. Int. Ed. 53 (2014) 1378–1381.
[4] C.C.L. McCrory, S.H. Jung, J.C. Peters, T.F. Jaramillo, Benchmarking heterogeneous electrocatalysts for the oxygen evolution reaction, J. Am. Chem. Soc. 135 (2013) 16977–16987.
[5] L. Zeng, T.S. Zhao, Integrated inorganic membrane electrode assembly with layered double hydroxides as ionic conductors for anion exchange membrane water electrolysis, Nano Energy 11 (2015) 110–118.
[6] C.L. Zhang, B.W. Wang, X.C. Shen, J.W. Liu, X.K. Kong, S.S.C. Chuang, D. Yang, A.G. Dong, Z.M. Peng, A nitrogen-doped ordered mesoporous carbon/graphene framework as bifunctional electrocatalyst for oxygen reduction and evolution reactions, Nano Energy 30 (2016) 503–510.
[7] Y.G. Li, P. Hasin, Y.Y. Wu, $Ni_xCo_{3-x}O_4$ nanowire arrays for electrocatalytic oxygen evolution, Adv. Mater. 22 (2010) 1926–1929.
[8] J. Wang, T. Qiu, X. Chen, Y.L. Lu, W.S. Yang, Hierarchical hollow urchin-like $NiCo_2O_4$ nanomaterial as electrocatalyst for oxygen evolution reaction in alkaline medium, J. Power Sources 268 (2014) 341–348.
[9] H.J. Shi, G.H. Zhao, Water oxidation on spinel $NiCo_2O_4$ nanoneedles anode: microstructures, specific surface character, and the enhanced electrocatalytic performance, J. Phys. Chem. C 118 (2014) 25939–25946.
[10] H. Hu, B.Y. Guan, B.Y. Xia, X.W. Lou, Designed formation of $Co_3O_4/NiCo_2O_4$ double-shelled nanocages with enhanced pseudocapacitive and electrocatalytic properties, J. Am. Chem. Soc. 137 (2015) 5590–5595.
[11] S. Chen, S.Z. Qiao, Hierarchically porous nitrogen-doped graphene–$NiCo_2O_4$ hybrid paper as an advanced electrocatalytic water-splitting material, ACS Nano 7 (2013) 10190–10196.
[12] W.Y. Xia, N. Li, Q.Y. Li, K.H. Ye, C.W. Xu, Au-$NiCo_2O_4$ supported on three-dimensional hierarchical porous graphene-like material for highly effective oxygen evolution reaction, Sci. Rep. 6 (2016) 23398, http://dx.doi.org/10.1038/srep23398.
[13] K.L. Pickrahn, S.W. Park, Y. Gorlin, H.B.R. Lee, T.F. Jaramillo, S.F. Bent, Active MnO_x electrocatalysts prepared by atomic layer deposition for oxygen evolution and oxygen reduction reactions, Adv. Energy Mater. 2 (2012) 1269–1277.
[14] L. Huang, D.C. Chen, Y. Ding, S. Feng, Z.L. Wang, M.L. Liu, Nickel–cobalt hydroxide nanosheets coated on $NiCo_2O_4$ nanowires grown on carbon fiber paper for high-performance pseudocapacitors, Nano Lett. 13 (2013) 3135–3139.
[15] A. Ramirez, P. Hillebrand, D. Stellmach, M.M. May, P. Bogdanoff, S. Fiechter, Evaluation of MnO_x, Mn_2O_3, and Mn_3O_4 electrodeposited films for the oxygen evolution reaction of water, J. Phys. Chem. C 118 (2014) 14073–14081.
[16] L. Zeng, T.S. Zhao, An effective strategy to increase hydroxide-ion conductivity through microphase separation induced by hydrophobic-side chains, J. Power Sources 303 (2016) 354–362.
[17] Y. Gorlin, T.F. Jaramillo, A bifunctional nonprecious metal catalyst for oxygen reduction and water oxidation, J. Am. Chem. Soc. 132 (2010) 13612–13614.
[18] H.Y. Jin, J. Wang, D.F. Su, Z.Z. Wei, Z.F. Pang, Y. Wang, In situ cobalt–cobalt oxide/N-doped carbon hybrids as superior bifunctional electrocatalysts for hydrogen and oxygen evolution, J. Am. Chem. Soc. 137 (2015) 2688–2694.
[19] X.K. Kong, C.L. Zhang, S.Y. Hwang, Q.W. Chen, Z.M. Peng, Free-standing holey Ni$(OH)_2$ nanosheets with enhanced activity for water oxidation, Small 13 (2017) 1700334.
[20] B. Chi, J.B. Li, Y.S. Han, Y.J. Chen, Effect of temperature on the preparation and electrocatalytic properties of a spinel $NiCo_2O_4$/Ni electrode, Int. J. Hydrog. Energy 29 (2004) 605–610.
[21] Z.L. Zheng, W.C. Geng, Y. Wang, Y. Huang, T. Qi, $NiCo_2O_4$ nanoflakes supported on titanium suboxide as a highly efficient electrocatalyst towards oxygen evolution reaction, Int. J. Hydrog. Energy 42 (2017) 119–124.